# Planar Blast Scaling with Condensed-Phase Explosives in a Shock Tube

Scott I. Jackson
Shock and Detonation Physics Group, Los Alamos National Laboratory,
Los Alamos, NM 87544

## 1 Introduction

Blast waves are strong shock waves that result from large power density deposition into a fluid. The rapid energy release of high-explosive (HE) detonation provides sufficiently high power density for blast wave generation. Often it is desirable to quantify the energy released by such an event and to determine that energy relative to other reference explosives to derive an explosive-equivalence value. In this study, we use condensed-phase explosives to drive a blast wave in a shock tube. The explosive material and quantity were varied to produce blast waves of differing strengths. Pressure transducers at varying lengths measured the post-shock pressure, shock-wave arrival time and sidewall impulse associated with each test. Blast-scaling concepts in a one-dimensional geometry were then used to both determine the energy release associated with each test and to verify the scaling of the shock position versus time, overpressure versus distance, and impulse.

Most blast scaling measurements to-date have been performed in a three-dimensional geometry such as a blast arena. Testing in a three-dimensional geometry can be challenging, however, as spherical shock-wave symmetry is required for good measurements. Additionally, the spherical wave strength decays rapidly with distance and it can be necessary to utilize larger (several kg) quantities of explosive to prevent significant decay from occurring before an idealized blast wave has formed. Such a mode of testing can be expensive, require large quantities of explosive, and be limited by both atmospheric conditions (such as rain) and by noise complaints from the population density near the test arena.

Testing is possible in more compact geometries, however. Non-planar blast waves can be formed into a quasi-planar shape by confining the shock diffraction with the walls of a shock tube. Regardless of the initial form, the wave shape will begin to approximate a planar front after successive wave reflections from the tube walls. Such a technique has previously been used to obtain blast scaling measurements in the planar geometry with gaseous explosives and the condensed-phase explosive nitroguanidine [1–3].

Recently, there has been much interest in the blast characterization of various non-ideal high explosive (NIHE) materials. With non-ideals, the detonation reaction zone is significantly larger (up to several cm for ANFO) than more ideal explosives. Wave curvature, induced by charge-geometry, can significantly affect the energy release associated with NIHEs. To measure maximum NIHE energy release accurately, it is desirable to minimize any such curvature and, if possible, to overdrive the detonation shock to ensure

Correspondence to: sjackson@lanl.gov 

completion of chemical reactions ahead of the sonic locus associated with the reaction zone. This is achieved in the current study through use of a powerful booster HE and a charge geometry consisting of short cylindrical lengths of NIHE initiated along the charge centerline.

## 2 Blast Scaling Theory

Blast scaling concepts were first developed almost a century ago [4] and understanding of the theory has been significantly improved since that time [5–7]. In this study, we consider the dimensionless group that characterizes the propagation of a shock front from an intense explosion [6].

$$\Pi = \frac{r}{\left(\frac{E}{\rho_0}\right)^{1/(2+\nu)} t^{(2/2+\nu)}} \tag{1}$$

The group is self-similar and consists of four variables: $E$, the source energy; $\rho_0$, the ambient atmospheric density; $r$, the distance of the shock front from the source; and $t$, the time from energy release. The parameter $\nu$ is a dimension-dependent index corresponding to 1, 2, or 3 for blast waves of planar, cylindrical, or spherical symmetry, respectively. The source energy accordingly has dimensions of $\mathsf{MT}^{-2}$, $\mathsf{MLT}^{-2}$, or $\mathsf{ML}^2\mathsf{T}^{-2}$ where $\mathsf{M}$ is mass, $\mathsf{L}$ is length, and $\mathsf{T}$ is time.

Proceeding in the planar geometry approximated by a quasi-planar shock propagating longitudinally inside a tube

$$r = \left(\frac{\alpha E}{\rho_0}\right)^{1/3} t^{2/3} \tag{2}$$

where the proportionality constant $\alpha = f(\nu, \gamma)$ and $\gamma$ is the atmospheric ratio of specific heats.

Differentiation with respect to time yields

$$U_s = \frac{2}{3}\sqrt{\frac{\alpha E}{\rho_0}}\frac{1}{\sqrt{r}} \tag{3}$$

where $U_s$ is the shock velocity.

For a strong shock ($M_s^2 \gg 1$) in a perfect gas,

$$\frac{P}{P_0} \rightarrow \frac{2\gamma}{\gamma+1} M_s^2 \tag{4}$$

where $M_s$ is the shock Mach number, $P_0$ is the ambient pressure, and $P$ is the post shock pressure. Equations 3 and 4 combine to form

$$P = \frac{8}{9}\left(\frac{1}{\gamma+1}\right)\left(\frac{\alpha E_0}{A}\right)\frac{1}{r} \tag{5}$$

Thus, the postshock pressure of a planar blast wave is inversely proportional to $r$. The planar energy $E$ has been replaced by the physical energy release $E_0$ (with the standard dimensions of $\mathsf{ML}^2\mathsf{T}^{-2}$) normalized by the cross-sectional area of the tube $A$. In this study, $\alpha$ is unity [6].

Figure 1: The shock tube.

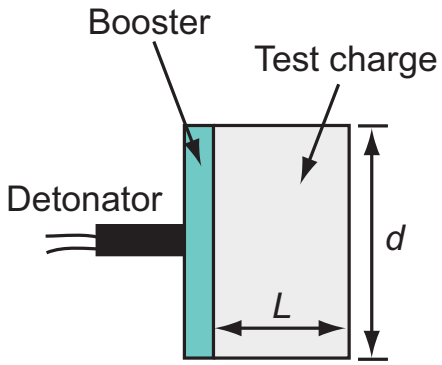


Figure 2: The axisymmetric charge geometry.

## 3 Experiment and Results

Data in the current study were obtained from tests in a shock tube with a 15.2-cm inner diameter and a length of 5.1 m. The working fluid was atmospheric air at Los Alamos atmospheric pressure (nominally 0.777 bar). Special consideration was used in the design to prevent plastic deformation of the facility due to the locally high-pressures near the condensed-phase detonation and to minimize the effect of structural noise on the measurements. Pressure transducers recorded the time-resolved shock overpressure as a function of distance and were located 0.64, 1.64, 2.64, 3.64, 4.64 and 5.04 m from the upstream end of the tube. The shock tube is shown inside of a blast chamber in Fig. 1.

Testing was performed for both ideal and non-ideal explosives. Ideal explosives tested included HMX-based PBX 9501 and PBX 9404, as well as RDX-based Composition 4 (C4) and PBX 9407. Non-ideal explosives tested included powdered, stoichiometric mixtures of potassium perchlorate ($KClO_4$) balanced with sugar ($C_{12}H_{22}O_{11}$), sodium perchlorate ($NaClO_4$) balanced with sugar, and ANFO (ammonium-nitrate-fuel-oil). Non-ideals were boosted (and significantly overdriven) by the PBX HEs. Explosive quantities fielded ranged from 2.5–51.0 g and at least three different masses of each charge were tested.

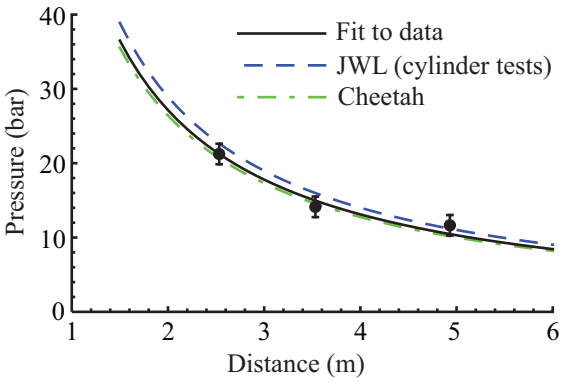


Figure 3: Comparison of Eq. 5 fit.

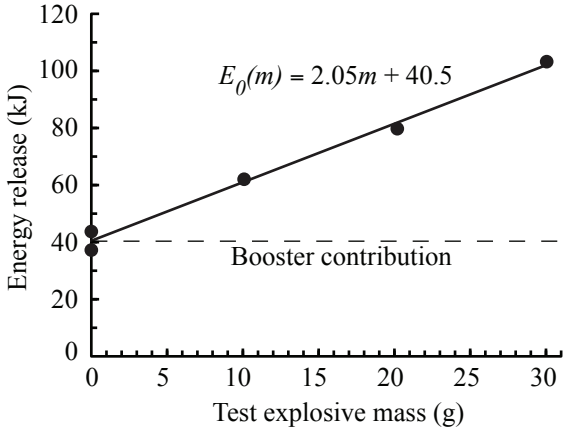


Figure 4: Determination of $\Delta H_{det}$ for an HE.

As some of the non-ideal mixtures were tested at diameters below their unconfined failure diameter limit, charges were formed into right cylinders with length-to-diameter ratios less than unity in order to prevent significant wave decay before the charge was consumed. Consoldiated charges were not confined and powdered ones were contained with a single layer of copy paper. The charge geometry is shown in Fig. 2. Additional details are given in Ref. 8.

For a given condensed-phase detonation in the shock tube, measurement of shock arrival times $t_s$ or $P$ versus $r$ along with Eqs. 2 or 5, respectively, allow determination of the released detonation energy $E_0$ that couples to the gas in the shock tube. In this study, $E_0$ values were derived from $P$ measurements. For a given test, Eq. 5 was fit to the peak $P$ values varying only $E_0$. The $E_0$ fit is shown for a 25g C4 shot in Fig. 3 and lies in between a prediction from the thermochemical code Cheetah and cylinder test experiments. For each explosive main charge series, identical boosters were used and linear fitting was then performed over all $E_0$ values to determine the specific energy or heat of detonation $\Delta H_{det}$ associated with the known booster and main charge masses ($NaClO_4$ data is shown in Fig. 4). The y-intercept of the fit corresponds to the booster energy, while the line slope was $\Delta H_{det}$ of the main charge. The experimentally measured $\Delta H_{det}$ values agreed well with accepted values for the PBX and C4 explosives obtained from calculation and other experiment. Additionally, all energy versus mass data fit well to a straight line (Fig. 4), indicating consistent $\Delta H_{det}$ measurements from test-to-test.

Since the flow is self-similar, experiments of different planar explosion lengths $E/P_0$ are expected to collapse together when nondimensionalized. Poor correlation or deviations from the theoretical curve indicate the failure of theoretical assumptions. Such an approach may seem circular, given that $E_0$ values were determined by fitting to theory. This is not the case, however. Each $E_0$ applies to all experimental $P$ data from a test, consisting of at least four measurements that were collected over a range of normalized distance $\bar{r}$. Thus, it is possible for specific $P$ values to not follow theory. It is also noted that the fit correlation shown in Fig. 4 is characteristic of all datasets, indicating little variation in the specific energies measured in each test.

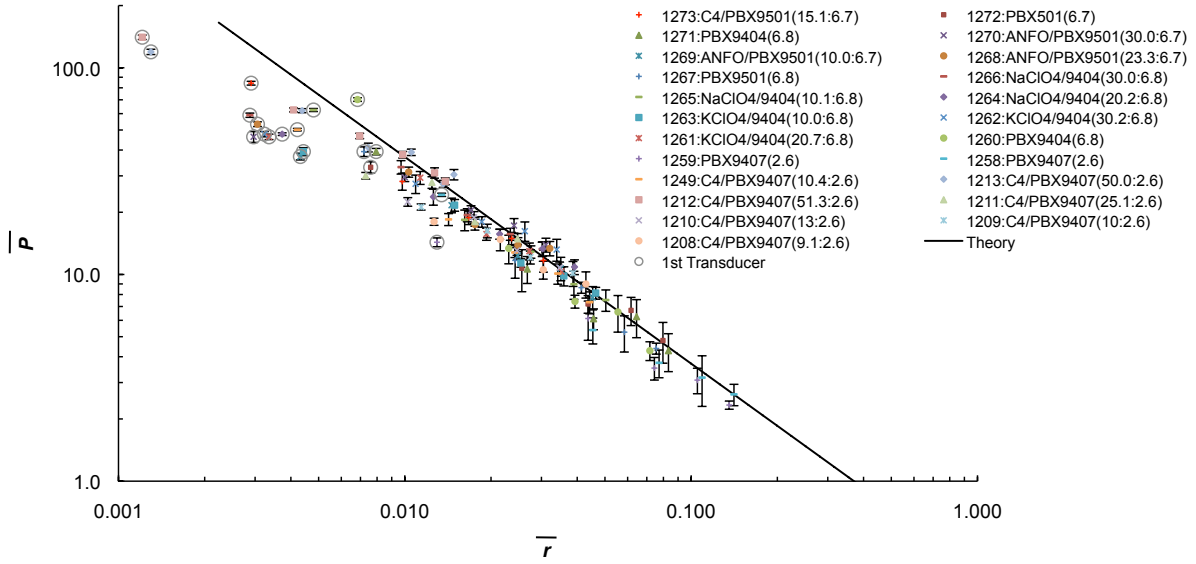


Figure 5: Nondimensional pressure versus distance.

Significant variation from theory will occur near the explosive source due to: (i) the finite CJ-pressure of the HE ($P \to \infty$ as $r \to 0$ for Eq. 5), (ii) the existence of a significantly non-planar front before sufficient wave-wall reflections have occurred near $r = 0$, (iii) the finite HE source size requiring shock-

steepening for a well-formed shock front (planar blast scaling theory assumes energy release along a plane of zero thickness), (iv) the "piston-effect" from the expansion of HE product gas, (v) and the breakdown of the perfect gas assumption at high temperature. These near-field effects will not scale with above theory and are best modeled numerically. Deviations in the far-field can also occur as the strong shock approximation is not longer met, requiring acoustic models [3].

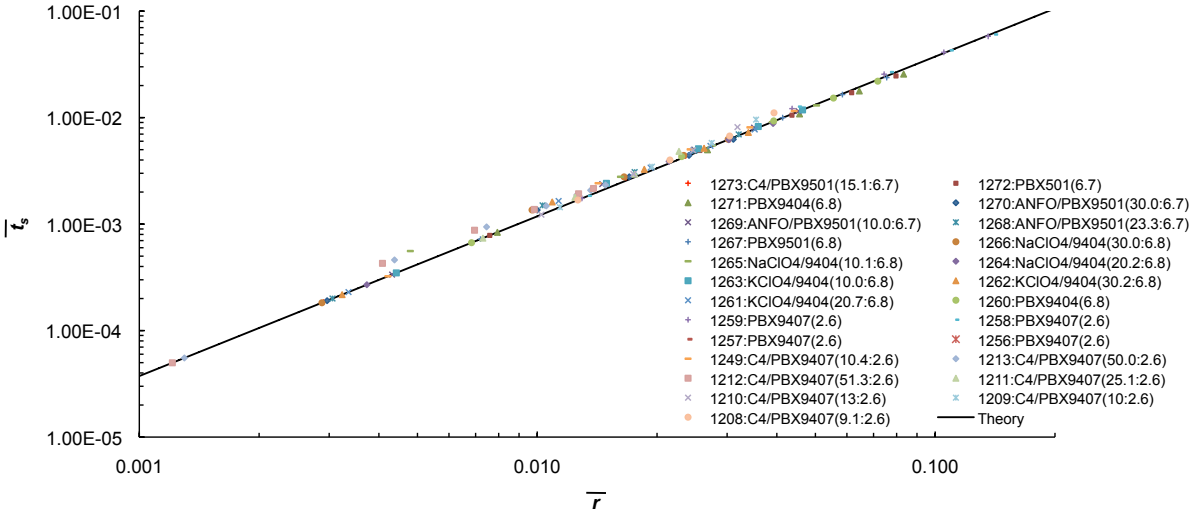


Figure 6: Nondimensional shock position versus time.

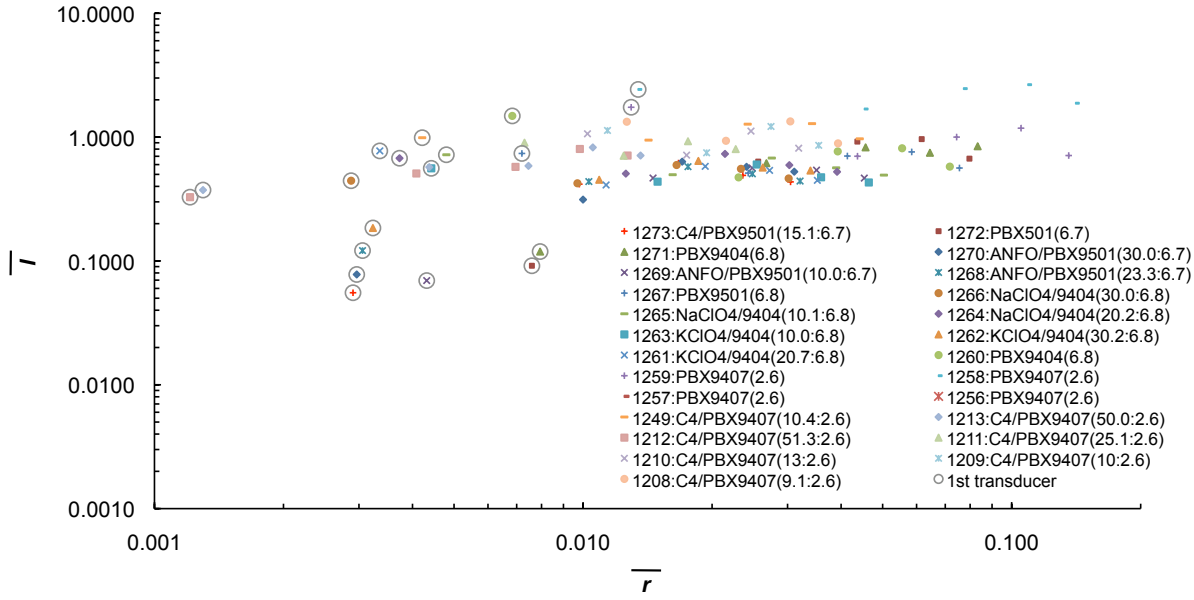


Figure 7: Nondimensional impulse versus distance.

The pressure correlation was previously demonstrated with a more limited data set [8]. Figure 5 contains additional pressure data and shows the nondimensional pressure $\bar{P} = \frac{\Delta P}{P_0}$, where $\Delta P = P - P_0$, versus nondimensional radius $\bar{r} = \frac{rP_0A}{E_0}$. The plot legend for each shot is of the form ⟨shot identification number⟩:⟨booster type⟩/⟨Main charge type⟩(⟨Booster mass in grams⟩:⟨Main charge mass in grams⟩).

The line is the expected data scaling from Eq. 5. The agreement between theory and experiment over most of the range is good, but for low values of $\bar{r}$, near-field effects become increasingly significant. Data from the transducer nearest the source (0.64m) are circled in grey to highlight this.

Shock position versus time is plotted in Fig. 6. The line corresponds to the expected scaling from Eq. 2. The nondimensional shock arrival time is $\bar{t_s} = \frac{t_s A}{E_0}\sqrt{\gamma\frac{P_0^3}{\rho_0}}$. The experimental data follows the theory well, but does exhibit slight deviations between $\bar{r}$ = 0.005–0.020, where experimental arrival times lag slightly behind theory.

Experimental impulse values are shown in Fig. 7 with normalized impulse $\bar{I} = \frac{IA}{E_0}\sqrt{\gamma\frac{P_0}{\rho_0}}$. Additional theory (not discussed) is required for an impulse scaling prediction, but the nondimensionalized experimental values do cluster to a value slightly below $\bar{I}$ = 1. As with the pressure measurements, there is significant variation in the near-field data for the first transducer location (circled). This is expected, since $I = \int P(t)dt$. Additionally, the piezoelectric transducers were not thermally protected from the hot postshock flow, so it is possible that thermally induced case expansion decreased the late time pressure and impulse readings. The above results, their correlation to blast scaling theory, as well as additional experiments and numerical calculations underway will be presented in more detail.

## References

[1] S. Ohyagi, E. Nohira, T. Obara, and P. Cai, "Propagation of pressure waves initiated by a flame and detonation in a tube," *JSME International Journal Series B*, vol. 45, no. 1, pp. 192–200, 2002.

[2] S. Ohyagi, T. Yoshihashi, and Y. Harigaya, "Direct initiation of planar detonation waves in methane/oxygen/nitrogen mixtures," in *Progress in Astronautics and Aeronautics*, pp. 3–22, AIAA, 1984. Presented in 1983 at the 9th International Colloquium on the Dynamics of Explosions and Reactive Systems (ICDERS).

[3] P. Thibault, J. Penrose, J. Shepherd, W. Benedick, and D. Ritzel, "Blast waves generated by planar detonations," in *Shock Tubes and Waves: Proceedings of the Sixteenth International Symposium on Shock Tubes and Waves*, pp. 765–771, Wiley VCH, 1988.

[4] B. Hopkinson, "British ordinance board minutes," tech. rep., 1915.

[5] G. Taylor, "The formation of a blast wave by a very intense explosion. I. theoretical discussion," *Proceedings of the Royal Society of London. Series A, Mathematical and Physical Sciences*, vol. 201, no. 1065, pp. 159–174, 1950.

[6] L. Sedov, *Similarity and Dimensional Methods in Mechanics, Tenth Edition*. CRC, 1993.

[7] R. Sachs, "The dependence of blast on ambient pressure and temperature," Tech. Rep. BRL Report 466, Aberdeen Proving Ground, Aberdeen, Maryland, 1944.

[8] S. Jackson, J. Morris, and L. Hill, "Determination of explosive blast loading equivalencies with an explosively driven shock tube," in *Proceedings of the APS Topical Group on Shock Compression of Condensed Matter*, vol. 1195, pp. 323–326, American Institute of Physics, 2009.